2022 IEEE/AIAA Transportation Electrification Conference and Electric Aircraft Technologies Symposium (ITEC+EATS) | 978-1-6654-0560-7/22/$31.00 ©2022 IEEE | DOI: 10.1109/ITEC53557.2022.9813959

Standstill Flux Linkage Measurement using Pulse Amplitude Modulated Current Injection towards Characterization of Interior Permanent Magnet Machines

Visweshwar Chandrasekaran[1], *Member, IEEE*, Bernard Jose[2], *Member, IEEE*, Petri Mäki-Ontto[3], *Member, IEEE*
Ned Mohan[*], *Life Fellow, IEEE, Kaushik Basu[$], Senior Member, IEEE,* Giri Venkataramanan[&], *Senior Member, IEEE*
Email: viswesh@umn.edu, bernard.jose@tranetechnologies.com, Petri.Maki-Ontto@tranetechnologies.com, mohan@umn.edu, kbasu@iisc.ac.in, giri@engr.wisc.edu
[1]Trane Technologies, St. Paul, MN, USA, [2]Trane Technologies, Bangalore, India, [3]Trane Technologies, Espoo, Finland
[*]Department of Electrical and Computer Engineering, University of Minnesota, Minneapolis, MN, USA
[$]Division of EECS, Indian Institute of Sciences, Bangalore, India
[&]Department of Electrical and Computer Engineering, University of Wisconsin, Madison, WI, USA

***Abstract*— This paper presents an experimental method for extraction of Direct (D) and Quadrature (Q) axis flux linkages of an Interior Permanent Magnet Synchronous Machine (IPMSM). The method considers both saturation and cross-magnetization effects over the entire range of the machine's rated current in both DQ axes. The flux-linkage characteristics are computed by exciting the stator windings through a series of current pulse injections via a switching converter using a closed-loop current regulator operating in a Field Oriented Control (FOC) scheme in the DQ frame. A novel method for generating the current pulse pattern is proposed which enables automatic creation of 2D Flux Linkage maps of the motor using any standard controller. The method takes advantage of standard measurements available in an industrial drive such as DC-link voltage, phase current, phase voltage and shaft position thus enabling the wide usage of the technique on industrial equipment for high-efficiency motor control algorithms. The proposed method in this paper achieves near standstill condition of any given test motor during pulse injections which enable experiments without the need for custom test rigs or isolation of motor from the shaft implements. Experimental results were taken on a 3HP IPMSM motor to validate the effectiveness of the proposed method.**

Keywords – parameter identification, cross-magnetization, flux-linkage measurement, interior permanent magnet synchronous machine (IPMSM), variable frequency drive (VFD)

I. INTRODUCTION

Permanent Magnet Synchronous Motors (PMSMs) are widely replacing traditional induction motors in many industrial applications while also being considered for modern high efficiency and power dense designs. A class of PMSMs with interior permanent magnets in rotors are purpose built to operate under high levels of magnetic saturation taking advantage of its saliency ratio [1-2]. Magnetic saturation of flux linkage in the self-axis as well the influence from the cross-axis is widely studied and reported in literature [2-5], [14-16]. There exist fundamental limitations in supplier generated datasheets for these machines which do not adequately specify the advanced non-linear properties. Knowledge of machine parameters is critical for accurate modelling of machines for design analysis as well as for developing high efficiency motor control algorithms.

To experimentally compute machine parameters, the academic literature proposes several methods for both standstill and rotational tests [6-11]. Rotational tests, while being popular and accurate, require a special test rig and an external prime mover for the Motor Under Test (MUT) [8,9]. Standstill tests can be performed on either a blocked or a free-to-spin rotor [6,7], [17-20]. Standstill techniques do not comprehensively map the motor's operating points and relies on extrapolation/curve fitting techniques [10]. While performing standstill tests rotor may have slight movement/low speed rotation as non-optimal $q-axis$ current injection may cause torque in the machine [10]. Most methods reported in literature can be grouped into either of these two categories - Pulsed Voltage (PV) injection or Pulsed Current (PC) injection. PV methods are limited by the sampling time of controller - practically around 25us for most applications [13]. For machines with higher time constants, longer PV duration can cause heating related drift in inductances and resistances. PC methods require an initial guess of motor parameters to tune the closed loop regulators. Since PC methods use DC current bias which may cause rotation in low inertia machines if the pulse duration is not carefully managed. The effect of inverter non-linearities need to be considered and the parameter identification techniques need to compensate for this. Based on these considerations, this paper identifies the below five evaluation criteria which enable wider adaptation of the parameter identification technique –

- C1: Method analyses the self and cross flux linkages for all operating points of the motor
- C2: Motor is at (near) standstill during the test
- C3: Motor is not required to be isolated from the load
- C4: Method does not require special power supplies, probes or data acquisition systems
- C5: Geometrical/FEA data of the machine is not required

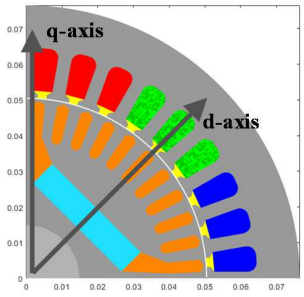

Fig. 1. Four Pole IPM geometry showing rotor magnet profile including rotor bars to aid in line-starting the machine

II. Mathematical Model of IPMSM

In this study, an IPMSM machine is considered whose mathematical expressions in the synchronous DQ frame are given by (1-5). The stator flux linkages have saturation properties that are influenced by both the self as well as cross-axis magnetizing currents, i.e., $\lambda_d(i_d, i_q)$ and $\lambda_q(i_d, i_q)$. These flux linkage maps were obtained via Finite Element Modelling of the IPMSM. For the given motor sample, a teardown analysis was performed to obtain key information of the stator and rotor geometries as seen in Fig. 1. Resulting 2D flux maps generated via FEA are shown in Fig. 2. An inverse map of DQ axis currents as a function of DQ flux linkages are also visualized.

$$v_q = R_s i_q + \frac{d\lambda_q}{dt} + \omega_e \lambda_d \quad (1)$$

$$v_d = R_s i_d + \frac{d\lambda_d}{dt} - \omega_e \lambda_q \quad (2)$$

$$T_{em} = T_{mag} + T_{rel} \quad (3)$$

$$T_{em} = \frac{3}{2}\frac{P}{2}\left(\lambda_d I_{qs} - \lambda_q I_{ds}\right) \quad (4)$$

$$\frac{d\omega_m}{dt} = \frac{1}{J}(T_{em} - T_{load}); \ \frac{d\theta_m}{dt} = \omega_m \quad (5)$$

As can be seen from the 2D maps, the flux linkages saturate with increasing magnitude of self-axis current while the cross-axis current also causes non-linear coupling causing additional saturation. This effect is more visible in the Q-axis flux which is described in much detail in [12]. The objective of this research is to develop a flux calculation method that excites the MUT with a current pulse pattern to construct the 2D flux maps with user's desired resolution and range.

III. Current Control Based Pulse Injection Principle

In this paper, the stator DQ flux linkages are calculated by exciting the MUT with a predetermined current pulse pattern. From (1) and (2) the voltage expressions for the IPMSM machine have three terms – IR voltage drop, differential flux and speed-volts. The last term can be neglected if the rotor is kept stationary with zero speed.

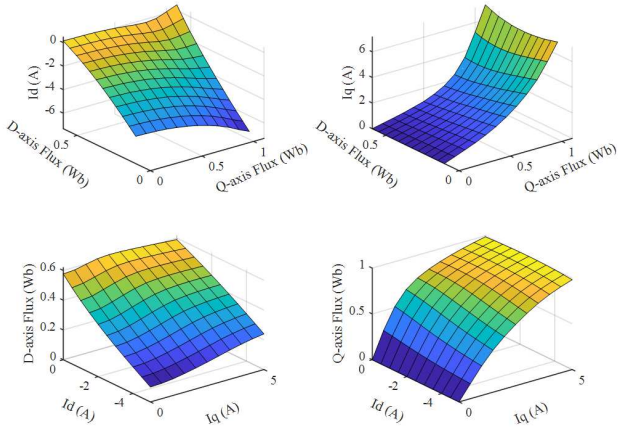

Fig. 2. $d-axis$ and $q-axis$ current vs flux relationships and inverse flux linkage maps generated via FEA simulations

This reduces the expressions to (6) and (7) which are re-written to compute flux linkages as an integral of the DQ applied voltage and response currents. The flux terms are a function of self and cross-coupled inductances as shown by (8) and (9).

$$\lambda_d = \int_0^t [v_d(\tau) - i_d(\tau)R_s]d\tau \quad (6)$$

$$\lambda_q = \int_0^t [v_q(\tau) - i_q(\tau)R_s]d\tau \quad (7)$$

Where,

$$\lambda_d = L_{dd}(i_d, i_q)i_d + L_{dq}(i_d, i_q)i_q \quad (8)$$

$$\lambda_q = L_{qd}(i_d, i_q)i_d + L_{qq}(i_d, i_q)i_q \quad (9)$$

A current pulse reference in the self-axis (say D) is created with a certain magnitude and width. Before the start of this pulse, a separate current pulse is generated, and its response allowed to settle in the cross-axis (say Q). This allows the calculation self-axis flux linkage with the cross-axis influence. The pulse amplitude for both self and cross-axes can be manipulated to get all combinations of currents. Similarly, the pulse duration can be managed to create steady state cross-axis DC current while the self-axis current is increased from zero. This logic is visualized in Fig. 3. For the experiments, we require measurements of motor currents, PWM voltage as well as DC-link voltage. Voltage sensing may be removed if adequate compensation is added to the commanded voltages considering the gain of the PWM modulation scheme, effect of deadtime and inverter losses.

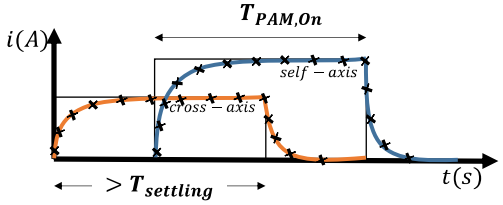

Fig. 3. Current pulse timing diagrams showing the placement of self and cross-axis current references

Careful considerations should be made to design the sampling rate of the measured current and voltages considering the machine's time constant and pulse duration which is well documented in [13].

IV. Proposed PAM Based DQ Current Reference Generation Scheme

The objective of this paper is to develop an automatic algorithm which is capable of exciting the MUT with a series of current pulses, which results in calculation of the DQ flux linkages under the influence of both $d-axis$ and $q-axis$ currents. The results of the automatic sequence are stored in a 2D array – one for $\lambda_d(i_d, i_q)$ and another for $\lambda_q(i_d, i_q)$. To achieve this, we take advantage of the concept of Pulse Amplitude Modulation (PAM). Two modulation signals are generated for the DQ current references. These are then compared with matching sampling signals at a frequency determined by the machine's time constant and bandwidth of the current regulators. Fig. 5 represents the PAM based pulse pattern to create a $[3x3]$ array for flux linkages. In the first part of the pattern for calculating $\lambda_q(i_d, i_q)$, the d-axis sampling signal leads q-axis by 90 degrees to allow for buildup of i_d ahead of exciting i_q. The black circles indicate the magnitude of the DQ current references which are sampled at the rising edge of sampling signals. The resultant pulse patterns will automatically help calculate the 2D flux maps. The PAM pulse current references generated through the proposed algorithm are then fed as input to a standard Field Oriented Control (FOC) control scheme with a current regulator. Triggering logic is created from the PAM generator to Sample and Hold the flux integration result at the last steady state point of each step response – for both rising and falling periods. These results are subsequently stored in the flux Look Up Table (LUT) arrays. This scheme is summarized in Fig. 6. The user has an option to provide input parameters such as the resolution of the flux maps, maximum allowable shaft rotation as well as estimated motor parameters.

The proposed method requires two independent current controllers. A key challenge in the design of the current regulator response is that the controller gains are dependent on the plant parameters being determined viz. saturated $d-axis$ and $q-axis$ inductances. By designing the controller to achieve critically damped response of the control signals (i_d and i_q) under the saturation range of inductances, it is possible to achieve accurate parameter determination. At the start of the test, a command pulse set to ~25% of rated current can be applied to calculate the machine's parameters such as resistance and inductance. This provides a reasonable estimate which can be used to tune the closed loop controllers.

The generated current references are in the form of short duration step pulses that reach up to peak rated current and the response time is determined by the closed loop regulator's bandwidth. While managing the step response of current there could be an overshoot in the DQ voltage commands given to the vector modulator. To avoid modulation index saturation, the controller's bandwidth needs to be carefully designed. As suggested in [13] a Pseudo Derivative Feedback (PDF) controller is chosen to minimize overshoot in the response. The transfer function, bandwidth and damping gains of the PDF controller are described in (10-11).

$$\frac{I(s)}{I_{ref}(s)} = \frac{1}{\frac{L}{K_i}s^2 + (\frac{R_s+K_p}{K_i})s+1} \tag{10}$$

$$\omega_{PDF} = \sqrt{\frac{K_i}{L}};\ \zeta_{PDF} = \frac{R_s+K_p}{2\sqrt{K_i L}} \tag{11}$$

Fig 4(a) and (b) show the closed loop bode and time domain response of the designed controller. Based on the mathematical model described in (1) and (2), the control system can be approximated to a first-order system while ignoring practical considerations such as inverter delay, sensor feedback delays and noise. As a case study, in Fig. 4(b) the IPMSM motor rated for 4A is simulated in MATLAB/Simulink. A step command is applied to the $q-axis$ current and tracking response of the PDF controller is studied. The test is repeated for different values of machine's inductance and the controller exhibits robustness in handling the parameter saturation.

Next, we determine the current pulse ON time duration whose lower limit is set to meet steady state tracking error of 2% and upper limit is set based on maximum allowable rotation in reaction to the pulse application. This results in an expression for $T_{PAM,On}$ $(= T_2 + T_3)$ given by (12). The total period is set to 5x the ON duration as a design practice to allow for steady state shaft settling (in case of rotation) and is given by (13). Corresponding to this, the inverter PWM frequency is set to acquire desired feedback samples per pulse period given by (14). This can further be designed to optimize the error in flux measurement for a given machine's time constant.

$$\frac{4}{\zeta_{PDF}\omega_{PDF}} < T_{PAM,On} < \sqrt{\frac{\theta_{m_{max}} J}{T_{em}}} \tag{12}$$

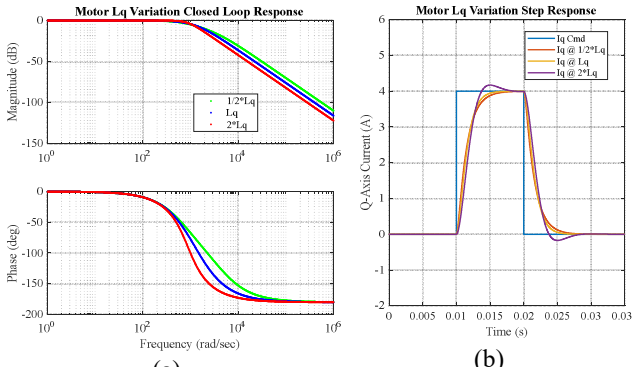

(a) (b)

Fig. 4. PDF controller robustness to inductance variation showing (a) frequency and (b) time responses

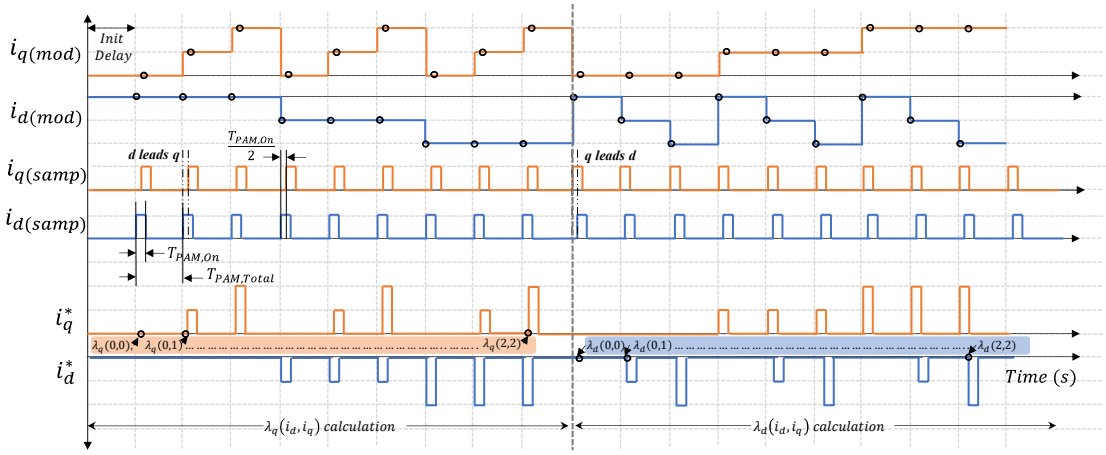

Fig. 5. Proposed Pulse Amplitude Modulated (PAM) Current Pulse Generation Scheme

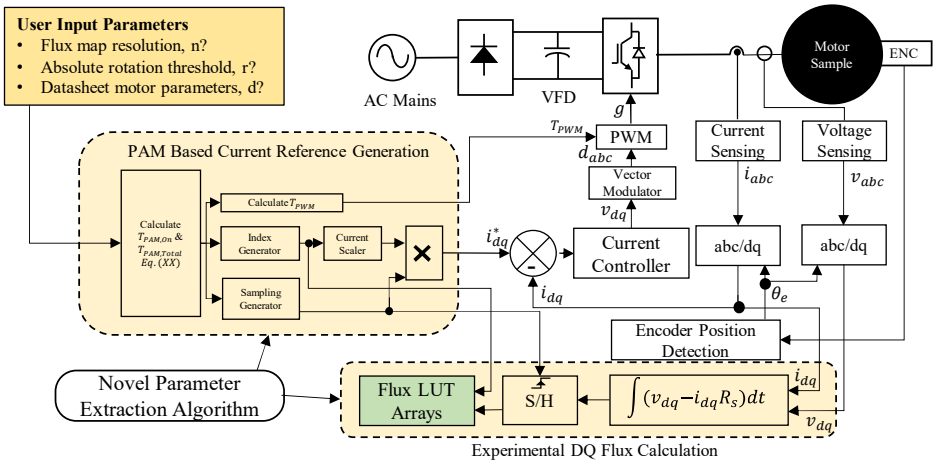

Fig. 6. Control Strategy for PAM based Pulse Current method using classic FOC scheme in DQ frame

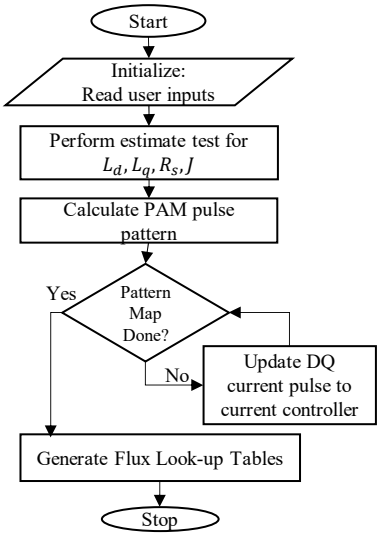

Fig. 7. Proposed parameter estimation flow diagram to calculate flux maps

$$T_{PAM,Total} = 5 * T_{PAM,On} \quad (13)$$

$$T_{PWM} < \frac{T_{PAM,Total}}{Sampling\ Resolution} \quad (14)$$

V. Simulation Study

MATLAB Simulink has been used to perform simulation studies on a 3 HP IPMSM MUT employing the proposed PAM based current injection algorithm to calculate the DQ flux linkages. The simulation is fully discretized with a base rate of $5\mu s$ to operate the switching inverter and motor subsystems. The machine's parameters are shown in Table I. Fig. 8(a) shows the sequential application of current pulses in both the $d-$ and $q-$ axes with corresponding DQ voltage pulses generated from the PDF controller given as input to the vector modulator for PWM generation. In order to calculate $q-axis$ flux the required i_d current is first established in the machine and under the presence of this the i_q current step is applied. Using the current pulse pattern, $q-axis$ flux tables are calculated during the interval $T = [0s - 10s]$ and $d-axis$ flux calculated between $T = [10s - 20s]$. Zoomed in regions shown in Fig. 8(b) and (c) demonstrate the current responses on application of pulse reference pattern reaching steady state within the pulse ON time.

The current regulators operate on the synchronous DQ current references generated through the proposed scheme. The output of the regulators are the command voltages, v_{dq}, which are given to a space vector modulator to generate the PWM gating pulses. A switching inverter based on classic 2-level Voltage Source Inverter (VSI) topology is implemented in simulation and switching frequency is set to $20kHz$. While optimizing the controller to manage the rise time of the currents, there will exist

an overshoot in the voltage command signals. Careful consideration must be made to limit the overshoot to under the DC bus utilization threshold. Hence, the on-pulse duration for the reference currents are influenced by the control bandwidth – further reinforcing the design rule identified in (12).

The corresponding flux linkages λ_d and λ_q are calculated through (6) and (7) during the transient period and the results are stored into the LUT arrays via the Sample and Hold logic shown in Fig. 6. FEA data shown in Fig 2 is used as ground truth to compare the calculated flux maps and relative % error is shown in Fig. 9. The results show a maximum error value of ~1.5% in the lower current regions. It is observed that the algorithm may introduce higher error while calculating flux maps in the low current regions owing to the practical limitations of feedback sensors and control gains at low magnitude of control signals.

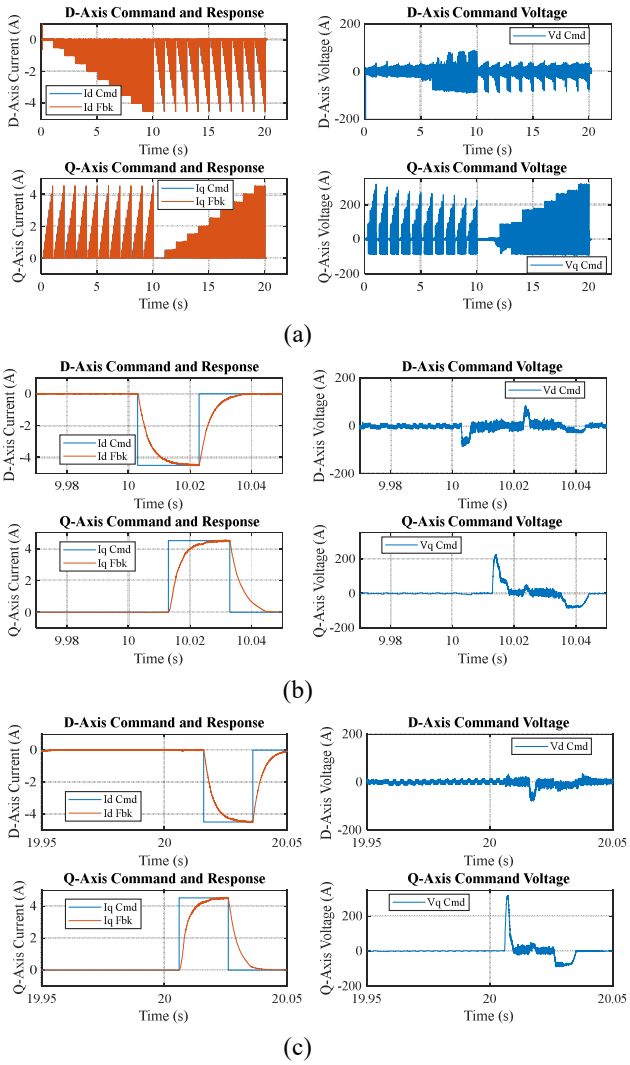

Fig. 8. DQ current and voltages applied to MUT for calculating DQ flux maps with (a) showing total pulse pattern lasting 20s for 3HP motor; (b) and (c) showing zoomed in regions of current and voltage waveforms for $\lambda_q(-4,4)$ and $\lambda_d(-4,4)$ respectively.

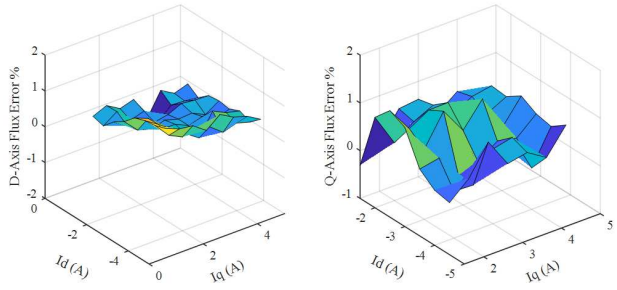

Fig. 9. Simulation result showing calculated DQ flux relative errors w.r.t FEA generated 2D maps

While applying the current pulse pattern to the motor sample, the rotor movement has been observed and reported in Fig. 10. The simulation was performed with a "free shaft" and a 3% load torque was applied to the motor model to account for shaft losses. This load torque would slightly dampen the mechanical rotation and represents the real-world test conditions. Results in Fig. 10(a) and (b) show the rotor movement during the $q-axis$ flux test ($T=[0s-10s]$) while (c) and (d) show the movement during the $d-axis$ test. As expected, the maximum rotor movement occurs at the full rated application of i_q which generates electromagnetic torque in the motor.

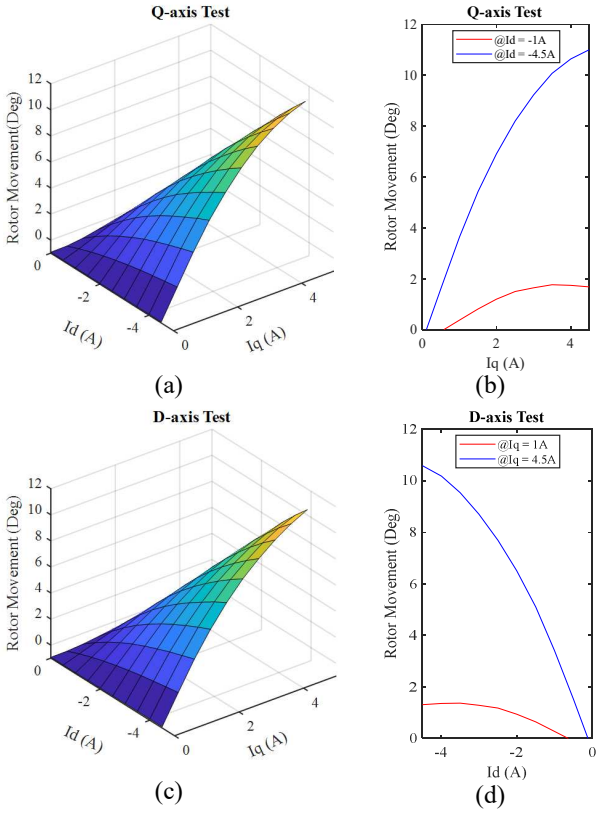

Fig. 10. Rotor movement visualized for (a), (b) $d-axis$ flux test and (c),(d) $q-axis$ flux test

VI. Control Scheme Realization on Embedded Target

The proposed PAM based current injection pattern has been developed using the Stateflow toolbox in MATLAB/Simulink. The timing sequence is synchronized with the PWM switching time step ($t_{sw} = 50\mu s$) and hence the $T_{PAM,On}$ and $T_{PAM,Total}$ are set to integral multiples of t_{sw} to ensure timing requirements and accuracy are met. It is desired to implement a discretized integration of (5) and (6) for flux calculation. A simple and practical method to realize this would be use the Forward Euler Discrete Integration method. The integrator scheme is triggered at each t_{sw} time step and accumulates the input signal. Since $t_{sw} \gg t_{PAM,On}$ the integration accuracy is very high. Design considerations have been made to implement anti-windup logic and prevent numeric overflow. The discrete integrator design is shown in Fig.11.

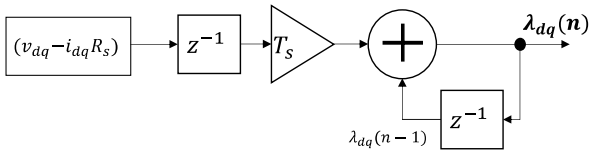

Fig. 11. Discrete Forward Euler Integrator for calculating flux

Fig. 7 presents the flowchart of the procedure and the logical sequence for real-time implementation. Flux maps can be generated at the desired user resolution which may elongate or shrink the total test period.

Timing diagram for the pulse reference current is shown in Fig. 12 and is also described in [13]. The period T_1 is used to remove DC offset errors from the measured currents and voltages. The flux linkages can be calculated for both the rising and falling periods of the currents (T_2, T_4) and an average of the two results can be calculated which doubles the accuracy. At the start of T_4 the reference current is reset back to zero. Since stator resistance, R_s can drift with temperature, it is beneficial to also measure this parameter during the steady state region of V and I, T_3. To remove inverter losses, a differential measurement can be used as described in [10] given by (15).

$$R_s = \frac{V_{dq2} - V_{dq2}}{I_{dq2} - I_{dq1}} \tag{15}$$

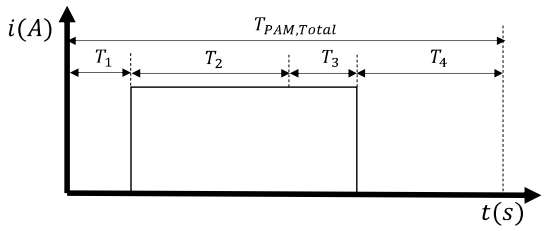

Fig. 12. Timing diagram showing the four unique calculation periods during the pulse period

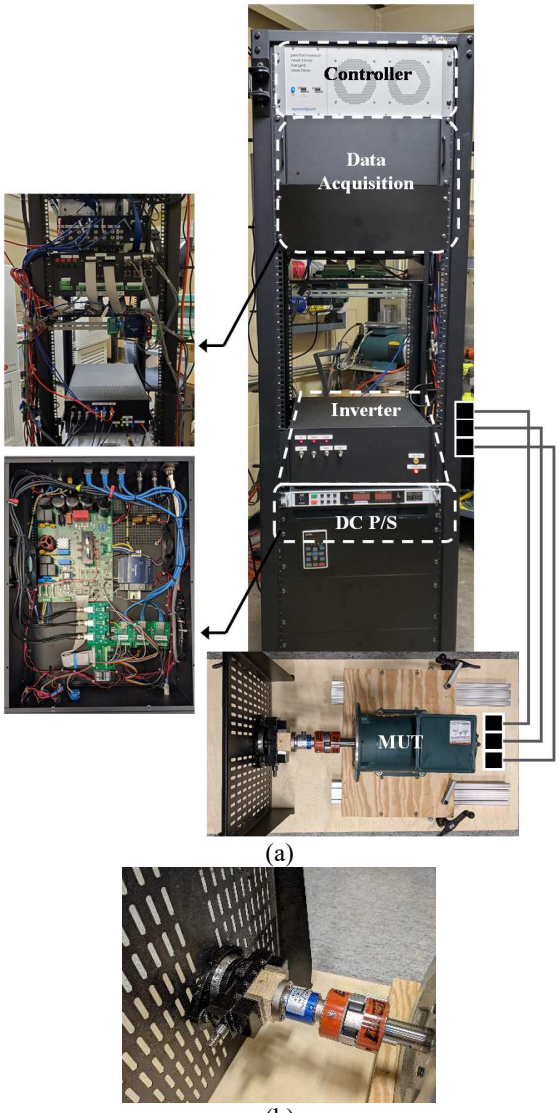

(a)

(b)

Fig. 13. Hardware setup (a) consisting of 7kW inverter module and 3HP IPMSM test rig with shaft coupled to a reaction torque sensor, and (b) zoomed in image showing shaft coupled to a rotating vise grip capable of locking with precise degree adjustments

TABLE I. IPM Motor Parameters From Vendor Datasheet

Parameter	Value
Rated Power	3 HP
Rated Voltage	460 $V - rms$
Rated Speed	1800 r/min
Rated Current	4 $A - rms$
Rated Torque	12 Nm
Stator Resistance, R_s	2.184 Ω
Direct Axis Inductance, L_d	10.393 mH
Quadrature Axis Inductance, L_q	300 mH
Magnet Flux Linkage, λ_{pm}	0.376 Wb
No. of Poles, P	4
Inertia, J	0.011 $kg.m^2$

VII. Experimental Setup and Results

In this section, experimental results are presented to demonstrate the accuracy of the flux calculation using the proposed current injection scheme. A model-based design approach has been taken using MATLAB/Simulink and auto-code generation tools have been used to generate the code. The code has been deployed on a Performance Real-Time target from Speedgoat. The Speedgoat controller consists of a 4.2 GHz Quad core Intel i7 CPU operating with Simulink Real Time operating system. The peripherals such as Analog, Digital I/O's as well as PWM are implemented on a Xilinx Kintex-7 FPGA option card called IO334 with a based clock rate of $10ns$. While this controller significantly exceeds the requirements of the proposed control scheme, the authors have taken advantage of the rapid prototyping capabilities offered by Speedgoat.

As seen in Fig. 13(a) a power inverter has been developed based on the classic 2-Level (2L) Voltage Source Inverter (VSI) topology. An evaluation board with P/N: EVAL-M5-IMZ120R-SIC has been sourced from Infineon Technologies for the power inverter. A custom data acquisition system has also been developed to measure various feedback quantities such as L-L PWM voltages, phase currents, DC bus voltage, shaft position, speed, and torque. The MUT used in this study is a 3HP IPM from Baldor with P/N: CSPM3611T with vendor provided datasheet is shown in Table I. A custom shaft locking mechanism has been invented as seen in Fig. 13(b). The mechanism uses a reaction torque sensor coupled to the motor shaft. The sensor is mounted onto a rotating vice grip which can be locked at precise angles. The test rig enables measurement of transient torque during pulse application while keeping the rotor locked. Two rounds of tests have been conducted –

- ❖ *Test 1:* Locked rotor test to measure motor's shaft torque introduced by the current injection scheme
- ❖ *Test 2:* Free-shaft test to measure rotor's angular movement during the current injection period.

The results of *Test 1* are presented in Fig. 14(d) which compares the instantaneous shaft torque between simulation and experiments performed on the motor. There exists a deviation in torque estimated via simulation and this is due to idealization of motor losses which are revealed in the hardware experiments.

Fig. 14(a) and (b) present experimental results for $\lambda_q(-4,4)$ and $\lambda_d(-4,4)$ respectively. By comparing these results with the simulated waveforms in Fig. 8(a) and (b) for identical conditions the following observations can be made –

- The PDF based current regulator behavior is consistent with simulation which confirms the performance of the controller to track control signal at the desired bandwidth and damping ratio.
- There exist practical issues such as zero current reference tracking which is generally challenging with

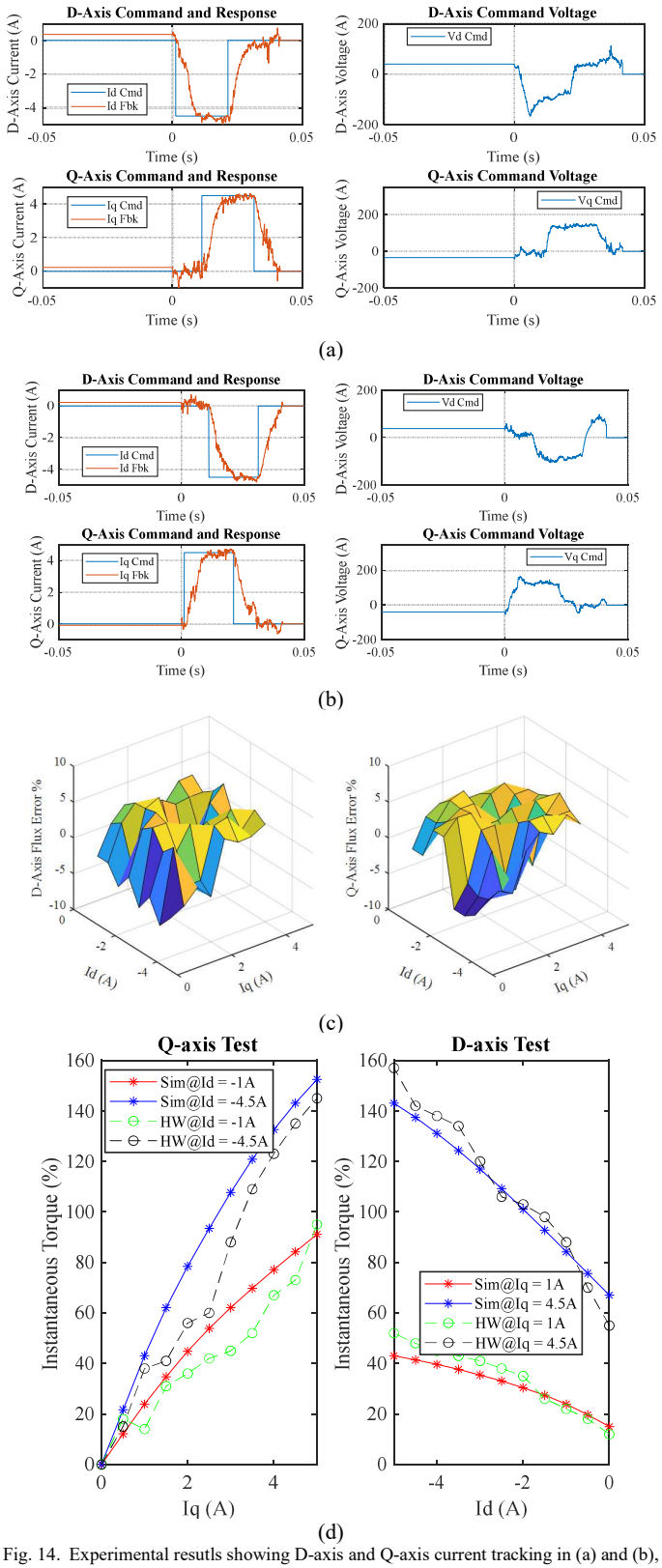

Fig. 14. Experimental resutls showing D-axis and Q-axis current tracking in (a) and (b), Current Space Vector in (c), Current Angle calculated via proposed MTPA algorithm in (d), Electromagnetic Torque estimated via controller a and load torque measured in (e) and 3 phase motor currents zoomed into a steady state region in (f)

a simple controller. Feedforward compensation may be added to aid the controller. Firmware modifications were made to minimize the zero current tracking period by adding PWM enable/disable logic between pulses

- Voltage command references generated by the controller have significant differences between simulation and hardware. This can be accounted by the fact that inverter non-linearities (e.g. deadtime, non-equal rise and fall times etc.) as well as feedback sensor noise exist in the real hardware which are idealized in simulation. The difference can be seen as simulation injecting a short overshoot voltage while hardware injecting a longer duration lower magnitude voltage to track command signal during the step response period. However, for the purpose of flux calculation, the area under the voltage curve remains consistent which can be confirmed by favorable levels of estimation errors as reported in Fig. 14(c).

While simulation results show flux estimation errors under 1% on average, the experimental estimation is achieved with ~5% average error. It is to be noted that the authors have implemented the proposed scheme on a 3 HP machine which has electrical time constant in the order of several milliseconds. A $20s$ test was determined to be optimal for this machine size. Larger machines naturally have much lower electrical time constants while having larger inertia. The proposed algorithm brings an advantage of lower test time for larger machines and this practically eliminates any temperature rise in the machine due to testing.

VIII. Conclusions

Modern requirements of advanced modelling and control of machines using drives demand an evolution of machine characterization methods. This requires accurate mapping of flux linkages while accounting for self and cross saturation properties of machine. This study proposes a novel current control-based pulse injection scheme to conveniently map the DQ axis flux linkages under the presence of both self and cross axis currents. The algorithm design is built around flexibility in controlling the magnitude and duration of the currents as well as the resolution of the 2D flux maps that are to be calculated. Flux calculation is achieved through a simple integral function while controlling the magnitude of shaft torque and hence rotor turn introduced by the test. Experimental results show predictable levels of instantaneous shaft torque which enables user to control the amount of rotor turn for the free-shaft standstill tests. This article presented design considerations for the current regulator considering system response requirements as well as parameter variation during operation due to saturation effects. Detailed simulation studies have been performed to characterize the effectiveness of the algorithm while achieving the five evaluation criteria identified at the beginning of the paper. Experimental calculation of flux linkages through the proposed method is compared with FEA data and very low relative error is reported showing the effectiveness of the scheme.

References

[1] Jahns, Thomas M., Gerald B. Kliman, and Thomas W. Neumann. "Interior permanent-magnet synchronous motors for adjustable-speed drives." IEEE Transactions on Industry Applications 4 (1986): 738-747.

[2] Sneyers, Brigette, Donald W. Novotny, and Thomas A. Lipo. "Field weakening in buried permanent magnet ac motor drives." IEEE Transactions on Industry Applications 2 (1985): 398-407.

[3] Vas, P., K. E. Hallenius, and J. E. Brown. "Cross-saturation in smooth-air-gap electrical machines." IEEE Transactions on Energy Conversion 1 (1986): 103-112.

[4] El-Serafi, A. M., and A. S. Abdallah. "Saturated synchronous reactances of synchronous machines." IEEE transactions on energy conversion 7.3 (1992): 570-579.

[5] Levi, Emil, and Viktor A. Levi. "Impact of dynamic cross-saturation on accuracy of saturated synchronous machine models." IEEE Transactions on Energy Conversion 15.2 (2000): 224-230.

[6] Stumberger, Bojan, et al. "Evaluation of saturation and cross-magnetization effects in interior permanent-magnet synchronous motor." IEEE Transactions on Industry Applications 39.5 (2003): 1264-1271.

[7] K. M. Rahman and S. Hiti, "Identification of machine parameters of a synchronous motor," IEEE Trans. Ind. Appl., vol. 41, no. 2, pp. 557–565, Mar./Apr. 2005

[8] E. Armando, R. I. Bojoi, P. Guglielmi, G. Pellegrino, and M. Pastorelli, "Experimental Identification of the Magnetic Model of Synchronous Machines," IEEE Transactions on Industry Applications, vol. 49, pp. 2116-2125, 2013.

[9] Pellegrino, Gianmario, Barbara Boazzo, and Thomas M. Jahns. "Magnetic model self-identification for PM synchronous machine drives." IEEE Transactions on Industry Applications 51.3 (2014): 2246-2254.

[10] Odhano, Shafiq Ahmed, et al. "Identification of the magnetic model of permanent-magnet synchronous machines using DC-biased low-frequency AC signal injection." IEEE Transactions on Industry Applications 51.4 (2015): 3208-3215.

[11] Cintron-Rivera, Jorge G., et al. "A simplified characterization method including saturation effects for permanent magnet machines." 2012 XXth International Conference on Electrical Machines. IEEE, 2012.

[12] Pellegrino, Gianmario, et al. The rediscovery of synchronous reluctance and ferrite permanent magnet motors: tutorial course notes. Springer, 2016.

[13] Thike, Rajendra, and Pragasen Pillay. "Automated current control method for flux-linkage measurement of synchronous reluctance machines." IEEE Transactions on Industry Applications 56.2 (2020): 1464-1474.

[14] "IEEE Trial-Use Guide for Testing Permanent Magnet Machines," in IEEE Std 1812-2014 , vol., no., pp.1-56, 24 Feb. 2015, doi: 10.1109/IEEESTD.2015.7047988.

[15] Pellegrino, Gianmario, et al. *The rediscovery of synchronous reluctance and ferrite permanent magnet motors: tutorial course notes*. Springer, 2016.

[16] Odhano, Shafiq Ahmed, et al. "Parameter identification and self-commissioning in AC motor drives: A technology status review." IEEE Transactions on Power Electronics 34.4 (2018): 3603-3614.

[17] Pescetto, Paolo, and Gianmario Pellegrino. "Sensorless standstill commissioning of synchronous reluctance machines with automatic tuning." 2017 IEEE International Electric Machines and Drives Conference (IEMDC). IEEE, 2017.

[18] Hinkkanen, Marko, et al. "Sensorless self-commissioning of synchronous reluctance motors at standstill without rotor locking." IEEE Transactions on Industry Applications 53.3 (2016): 2120-2129.

[19] Pescetto, Paolo, and Gianmario Pellegrino. "Determination of PM Flux Linkage Based on Minimum Saliency Tracking for PM-SyR Machines Without Rotor Movement." IEEE Transactions on Industry Applications 56.5 (2020): 4924-4933.

[20] Wiedemann, Simon, and Ralph M. Kennel. "Encoderless self-commissioning and identification of synchronous reluctance machines at standstill." 2017 IEEE 26th International Symposium on Industrial Electronics (ISIE). IEEE, 2017.